

Extended Object Tracking Based on Gaussian Process in Non-Gaussian Noise Environment

Lifan Sun^{1,2,3*} , Yongning Wang¹ , Dan Gao¹ 

1. Henan University of Science and Technology  – School of Information Engineering – Luoyang – China.

2. Longmen Laboratory – Luoyang – China.

3. Henan Academy of Sciences  – Zhengzhou – China.

*Correspondence author: lifan.sun@gmail.com

ABSTRACT

Extended object tracking (EOT) is a prominent research area in high-resolution radar surveillance, ship tracking, and video tracking. However, EOT algorithms are susceptible to non-Gaussian noise from factors such as sensor performance and environmental conditions. To address this problem, the Gaussian process (GP)-based maximum correntropy criterion square root cubature Kalman filter algorithm (GP-MCC-SRCKF) for EOT in non-Gaussian noise environments is proposed in this paper. The proposed method utilizes a GP to model extended objects, thereby enhancing estimation accuracy. Furthermore, weighted least squares (WLS) and MCC are incorporated to construct a cost function. The proposed method considers high-order moments of estimation error and effectively handles outliers in non-Gaussian noise environments. MCC-SRCKF improves the accuracy of object state estimation in non-Gaussian noise environments while ensuring the positive definiteness and symmetry of the error covariance matrix. Finally, simulation experiments are conducted to demonstrate the effectiveness of the proposed method.

Keywords: Gaussian process; Extended object tracking; Maximum correntropy criterion; Non-Gaussian noise.

INTRODUCTION

The advancement of high-resolution sensor technology has led to the widespread application of extended object tracking (EOT) in various civil and military domains, such as high-resolution radar, ship tracking, and autonomous driving (Kunz *et al.* 2015; Thormann *et al.* 2018; Zhou *et al.* 2019). Compared with traditional point target tracking, EOT presents many new challenges. First, a single object can generate multiple random scattering points during a single scanning cycle, resulting in multiple measurements. Second, besides the kinematic states, the contour states of the extended object also need to be taken into account (Granström *et al.* 2017).

Several EOT algorithms have been proposed to address these challenges. For example, Koch proposed the random matrices (RM) method (Koch 2008), which approximates the extended object as an ellipse and represents it using a positive definite RM. This method employs the Gaussian distribution probability density function (PDF) to describe the object's kinematic state and the inverse Wishart distribution PDF to describe its contour state within a Bayesian filtering framework. However, Koch's RM model does not consider sensor noise, leading to decreased accuracy in shape estimation for extended objects. Subsequently, Feldmann improved Koch's measurement model by considering the impact of measurement noise on object shape estimation and clarifying the relationship between measurement variance and RM variables (Feldmann *et al.* 2010; Feldmann and Koch 2012). However, this RM method assumes an elliptical shape for the extended object, which may not always hold true in practical applications (Baum and Hanebeck 2012). To address this limitation, Lan Jian proposed the multi-ellipse RM method (Lan and Li 2014; Zong and Barbary 2015), which represents non-elliptical extended

Received: Apr. 10, 2024 | **Accepted:** Oct. 10, 2024

Section editor: Paulo Renato Silva 

Peer Review History: Single Blind Peer Review.



objects or group objects as a combination of multiple elliptical sub-objects, thereby obtaining higher estimation accuracy compared to a single elliptical model. However, this approach greatly increases the algorithm's complexity and computational requirements. Baum and Hanebeck (2014) established the random hypersurface model (RHM) method and employed nonlinear filtering to estimate the object state. This model can describe elliptical objects and estimate any complex extended form, such as star convexity. However, when the approximate value of the radial function in the RHM model is negative, it can lead to unpredictable estimation results and a decrease in tracking accuracy (Sun *et al.* 2012). An improved RHM model that can effectively avoid the problem of shape divergence has been proposed (Sun *et al.* 2022); however, there is room for further improvement in estimation accuracy.

Gaussian process (GP) is a stochastic process composed of infinite-dimensional normal distribution functions and is widely used in machine learning (Osborne and Osborne 2010). Wahlström used the GP method to model measurements and track extended objects (Wahlström and Özkan 2015), and combined the model with the extended Kalman filter (EKF) to address the EOT problem of star convex shapes under ideal conditions. Subsequently, various GP-based algorithms for EOT have been proposed, with some studies (Ebert and Wuensche 2019; Kumru and Özkan 2018; 2021) extending their results from two-dimensional to three-dimensional space. A spatiotemporal GP model for EOT has been proposed to track non-rigid and asymmetric extended objects (Aftab *et al.* 2019). To achieve EOT in complex backgrounds, the GP-based probabilistic data association algorithm was proposed (Guo *et al.* 2018), and the posterior Cramer-Rao lower bound was derived to evaluate EOT performance with measurement origin uncertainty. Combining GP with a labeled multi-Bernoulli filter was proposed in a previous study (Hirscher *et al.* 2016) to address data association for multiple extended objects.

GP models demonstrate superior capabilities in learning irregular shapes in real-time, enabling them to estimate more complex and variable contours of extended objects compared with RM and RHM methods. However, most existing studies on GP models for EOT algorithms assume Gaussian noise distribution, disregarding the potential effects of non-Gaussian noise on the system. Practical radar systems can be affected by various factors, such as environmental disturbances and momentary faults in sensors, leading to outliers in measurements. Moreover, the unpredictable high maneuverability of objects introduces outliers in the process noise. These factors result in process and measurement noise exhibiting heavy-tailed characteristics, deviating from the assumption of a Gaussian distribution (Zhu *et al.* 2020; 2021). Employing traditional object tracking algorithms that assume Gaussian white noise would considerably degrade the tracking performance and potentially lead to tracking failure. Therefore, considering process noise and measurement noise as non-Gaussian distributions is more aligned with practical scenarios.

Numerous algorithms have been developed to address object tracking in the presence of non-Gaussian noise. For example, an improved particle filtering algorithm has been proposed to accurately estimate the object state and parameters in the presence of complex noise and sensor faults (Zhu *et al.* 2019). However, particle filtering requires a large number of samples to approximate the posterior probability density of the system; this greatly increases the complexity of the algorithm. In recent years, the correntropy criterion in information theory learning has received increased attention and has been widely used in many signal processing and machine learning applications (Lv *et al.* 2021). The maximum correntropy criterion (MCC) generated by the correntropy property is used as a local similarity measure mainly to analyze signals affected by outliers, reduce the influence of outliers on the estimation results, and provide robust and reliable analysis results. Compared with traditional methods, it is not affected by the assumption of Gaussian distribution and is more suitable for non-Gaussian systems in the presence of non-Gaussian noise. A Kalman filter based on the MCC has been proposed (Chen *et al.* 2017; Izanloo *et al.* 2016). It can obtain second-order information about the error and capture high-order statistics of the filtering error, thus greatly improving the tracking performance and robustness of the system. However, this method has not been employed for EOT. Compared with the minimum mean square error optimization criterion, the MCC exhibits significant superiority, especially when dealing with error distributions containing outliers and non-zero means (Liu *et al.* 2007).

For EOT in non-Gaussian noise environments, an efficient method is proposed in this paper. The main innovations are concluded as follows:

- In this paper, GP is used to model the object extent. This method describes the radial function of the object shape based on the learning characteristics of GP, and can model the complex and changeable extended object contour more flexibly.
- Due to the rarity of ideal Gaussian noise in practical tracking scenarios, a non-Gaussian noise model is introduced to describe the real noise distribution characteristics as accurately as possible.

- Unlike existing EOT algorithms, the high-order statistics of the error are fully utilized in this approach, which helps to reduce the influence of noise and improve tracking performance.

The remainder of this paper is organized as follows. First, an overview of GP regression is provided. Next, the GP-based extended target tracking algorithm in non-Gaussian noise environments is discussed, and a square root cubature Kalman filter (SRCKF) algorithm based on MCC is proposed to address non-Gaussian noise. The simulation results are then presented in the simulation experiments and discussions. Finally, conclusions are presented.

Gaussian process regression

A GP is a random process consisting of an infinite number of normally distributed random variables, where any finite combination of random variables is a multivariate Gaussian distribution. Gaussian process (GP) is uniquely defined with its mean function $\mu(u)$ and covariance function $k(u,u')$ of a function as:

$$\begin{aligned} \mu(u) &= E[f(u)] \\ k(u, u') &= E[(f(u) - \mu(u))(f(u') - \mu(u'))^T] \end{aligned} \tag{1}$$

and the GP is denoted as:

$$f(u) \sim GP(\mu(u), k(u, u')) \tag{2}$$

where u is the function input.

Given a finite set of inputs u_1, \dots, u_N , the corresponding outputs $f(u_1) \dots f(u_N)$ are jointly decided by the mean and covariance function:

$$\begin{bmatrix} f(u_1) \\ \vdots \\ f(u_N) \end{bmatrix} \sim N(\mu, K) \tag{3}$$

where:

$$\mu = \begin{bmatrix} \mu(u_1) \\ \vdots \\ \mu(u_N) \end{bmatrix}, K = \begin{bmatrix} k(u_1, u_1) & \dots & k(u_1, u_N) \\ \vdots & \ddots & \vdots \\ k(u_N, u_1) & \dots & k(u_N, u_N) \end{bmatrix} \tag{4}$$

The covariance function is a crucial component of a GP and is commonly represented by the squared exponential covariance function, which is defined as follows:

$$k(u, u') = \sigma_f^2 e^{-\frac{2 \sin^2\left(\frac{u-u'}{2}\right)}{l^2}} + \sigma_r^2 \tag{5}$$

where σ_r and σ_f represent the prior variables of the mean radius and contour radius function, respectively, and l represents the scale factor.

The GP model is primarily used to incorporate training data to learn an unknown function. Considering the measurement function as follows:

$$z_k = f(u_k) + e_k, \quad e_k \sim N(0, R) \tag{6}$$

where z_k is the measurement that function $f(\cdot)$ contains noise when the training input is u_k , e_k is the measurement noise, and R is the covariance of the measurement noise.



The learning process is mainly as follows: given a set of measurements $\mathbf{z} = [z_1, \dots, z_N]^T$ and their corresponding input $\mathbf{u} = [u_1, \dots, u_N]^T$, the function $f(\cdot)$ is learned through GP, so that when the input is $\mathbf{u}^f = [u_1^f, \dots, u_{N_f}^f]^T$, the corresponding function value $\mathbf{f} = [f(u_1^f), \dots, f(u_{N_f}^f)]^T$ can be estimated according to the learned function.

In object tracking, all the measurements may not be available as a batch, but they might be collected sequentially over time. Second, the complexity of the regression problem increases cubically with the number of measurements, which is not feasible for an online implementation. Therefore, the aim is to achieve an approximate recursive update of the posterior. According to the derivation in (Wahlström and Özkan 2015), the joint distribution for the measurements z_k and the function values \mathbf{f} is:

$$\begin{bmatrix} z_k \\ \mathbf{f} \end{bmatrix} \sim N \left(\mathbf{0}, \begin{bmatrix} K(u_k, u_k) + R & K(u_k, \mathbf{u}^f) \\ K(\mathbf{u}^f, u_k) & K(\mathbf{u}^f, \mathbf{u}^f) \end{bmatrix} \right) \quad (7)$$

In this work, mean function is set to zero-valued. From the joint Gaussian distribution $p(\mathbf{z}, \mathbf{f})$ in Eq. 7, the likelihood and the initial prior can easily be computed as:

$$p(z_k | \mathbf{f}) = N(z_k; H_k^f \mathbf{f}, R_k^f) \quad (8)$$

$$p(\mathbf{f}) = p(\mathbf{0}, P_0^f) \quad (9)$$

with:

$$H^f(u_k) = K(u_k, \mathbf{u}^f) [K(\mathbf{u}^f, \mathbf{u}^f)]^{-1} \quad (10)$$

$$R^f(u_k) = K(u_k, u_k) + R - H^f(u_k) K(\mathbf{u}^f, u_k) \quad (11)$$

$$P_0^f = K(\mathbf{u}^f, \mathbf{u}^f) \quad (12)$$

By exploiting the structure of this likelihood, a state space model is constructed, which enables the application of the Kalman filter for recursive GP regression:

$$\mathbf{x}_{k+1}^f = F^f \mathbf{x}_k^f + w_k, \quad w_k \sim N(\mathbf{0}, Q^f) \quad (13)$$

$$\mathbf{z}_k = H^f(u_k) \mathbf{x}_k^f + e_k^f, \quad e_k^f \sim N(\mathbf{0}, R^f(u_k)) \quad (14)$$

$$\mathbf{x}_0^f \sim N(\mathbf{0}, P_0^f) \quad (15)$$

where:

$$\mathbf{x}_k^f = \mathbf{f} = [f(u_1^f), \dots, f(u_{N_f}^f)]^T \quad (16)$$

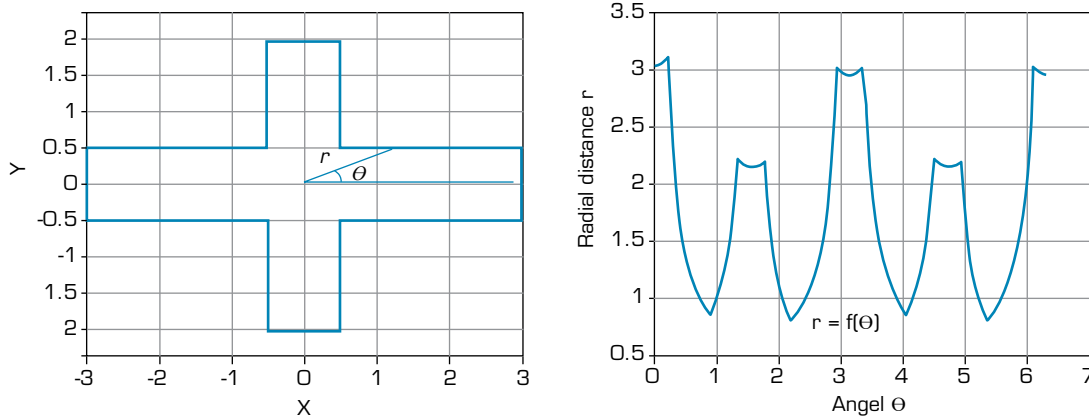
$$F^f = e^{-\alpha T} I \quad (17)$$

$$Q^f = (1 - e^{-2\alpha T}) K(\mathbf{u}^f, \mathbf{u}^f) \quad (18)$$

where x_k^f is interpreted as the contour state of the extended target, F^f represents the transition matrix of contour state and Q^f is the process noise covariance, and T is the sampling time. The parameter $\alpha \geq 0$ will determine the speed of contour evolution and can be considered a forgetting factor.

Extended object tracking (EOT) algorithm based on GP in non-Gaussian noise environment

The planar star-convex shape of the set $E(x)$ is a star-convex shape if the set consisting of at least one point m in the set $E(x) \subset Y^2$ and all points on the line of any point X in the set is still a subset of the set. For ease of calculation, the radial function $r = f(\theta)$ is used to describe the star-convex shape, as shown in Fig. 1.



Source: Elaborated by the authors.

Figure 1. Description of planar star-convex shapes using a radial function $r = f(\theta)$. (a) star-convex, extent shape; (b) radial function.

Extended object model under GP regression

Motion model

Under the extended object model based on GP, the object state at time k is represented as follows:

$$x_k = \left[\bar{x}_k^T \ (x_k^f)^T \right]^T = \left[(x_k^c)^T \ \varphi_k \ (x_k^*)^T \ (x_k^f)^T \right]^T \tag{19}$$

where x_k^c represents the position of the object centroid, φ_k represents the orientation of the object, and x_k^* represents the optional additional state of the object (velocity and angular velocity). x_k^f represents the contour state of the object, which is composed of a series of function values of the extended object radial function at equidistant sampling points in interval $[0, 2\pi]$. Therefore, the extended object state consists of two parts: kinematic state \bar{x}_k and contour state x_k^f :

The kinematic state transition equation for object state $\bar{x}_k = \left[(x_k^c)^T \ \varphi_k \ (x_k^*)^T \right]^T$ is:

$$\bar{x}_{k+1} = \bar{F}\bar{x}_k + \bar{w}_k \tag{20}$$

where \bar{F} represents the transition matrix of kinematic state and \bar{w}_k is the process noise with the covariance matrix \bar{Q}_k .

Together with the dynamical description of the object extent in Eq. 13, an augmented description of the dynamics is constructed:

$$x_{k+1} = Fx_k + w_k \tag{21}$$

where:

$$x_k = \begin{bmatrix} \bar{x}_k \\ x_k^f \end{bmatrix}, \quad F = \begin{bmatrix} \bar{F} & 0 \\ 0 & F^f \end{bmatrix}, \quad Q_k = \begin{bmatrix} \bar{Q} & 0 \\ 0 & Q^f \end{bmatrix} \tag{22}$$



where F^f and Q^f are defined in Eqs. 17 and 18. The matrices \bar{F} and \bar{Q}_k are given later in the simulation section.

Measurement model

The star-convex model is usually used to describe an extended object, and the learning characteristics of GP regression are integrated to estimate the shape of the extended object. Owing to the definition of the star-convex model, an object's shape can be characterized by the radius function $r = f(\theta)$. When the measurement obtained by the sensor originates from the object surface, the measurement equation is expressed as follows:

$$z_{k,l} = x_k^c + s_{k,l} p(\theta_{k,l}) f(\theta_{k,l}) + e_{k,l} \quad (23)$$

where x_k^c represents the position of the object centroid at time k , $\{z_{k,l}\}_{l=1}^{n_k}$ represents the n_k measurements obtained at time k , $\{\theta_{k,l}\}_{l=1}^{n_k}$ represents the angle describing the origin of these measurements on the object contour. The scalar $s_{k,l} \in [0, 1]$ is a random scaling factor, where under the assumption that the measurement points are uniformly distributed over the object surface, the scaling factor $s_{k,l}$ satisfies $s_{k,l} \sim N(\mu_s, \sigma_s^2)$. $p(\theta_{k,l})$ is defined as the direction vector, $e_{k,l}$ represents the measurement noise with covariance matrix $R_{k,l}$. The radius function $r = f(\theta)$ of the object contour can be learned through a GP, i.e.,

$$f(\theta) \sim GP(\mu(\theta), K(\theta, \theta')) \quad (24)$$

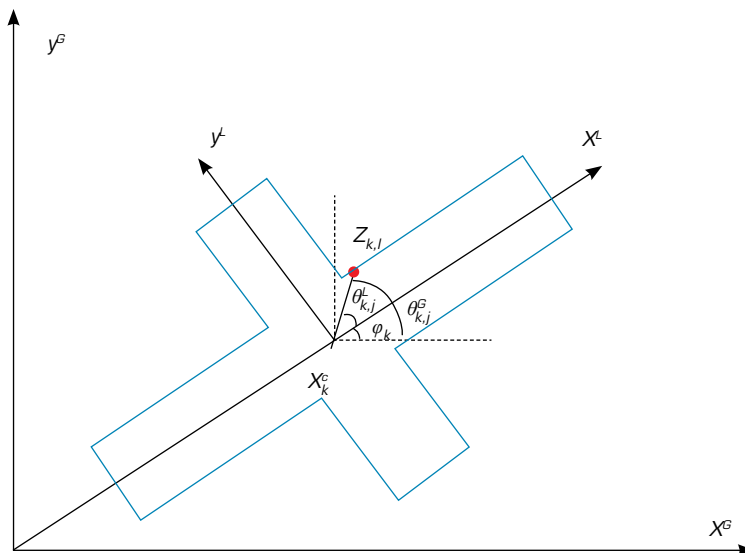
Each measurement $z_{k,l}$ is associated with an angle $\theta_{k,l}^G$ that depends on its angular location relative to the object position x_k^c :

$$\theta_{k,l}^G(x_k^c) = \angle(z_{k,l} - x_k^c) \quad (25)$$

This angle can also be described in the local object coordinate frame using the object orientation state φ_k :

$$\theta_{k,l}^L(x_k^c, \varphi_k) = \theta_{k,l}^G(x_k^c) - \varphi_k \quad (26)$$

The graphical illustration of this geometry is shown in Fig. 2.



Source: Elaborated by the authors.

Figure 2. Measurement model of an object with an orientation of φ_k .

After introducing the angle, a more detailed expression can be provided through Eq. 23:

$$z_{k,l} = x_k^c + s_{k,l} p_{k,l} \left(x_k^c \right) f \left(\theta_{k,l}^L \left(x_k^c, \varphi_k \right) \right) + e_{k,l} \quad (27)$$

Meanwhile, the direction vector can be represented as:

$$p_{k,l} \left(x_k^c \right) = p \left(\theta_{k,l}^G \left(x_k^c \right) \right) = \frac{z_{k,l} - x_k^c}{\left\| z_{k,l} - x_k^c \right\|} \quad (28)$$

According to the recursive form of GP regression described in the Gaussian process regression section, Eq. 27 can be further derived as:

$$\begin{aligned} z_{k,l} &= x_k^c + s_{k,l} p_{k,l} \left(x_k^c \right) f \left(\theta_{k,l}^L \left(x_k^c, \varphi_k \right) \right) + e_{k,l} \\ &= x_k^c + s_{k,l} p_{k,l} \left(x_k^c \right) \left[H^f \left(\theta_{k,l}^L \left(x_k^c, \varphi_k \right) \right) x_k^f + e_{k,l}^f \right] + e_{k,l} \\ &= x_k^c + s_{k,l} p_{k,l} \left(x_k^c \right) H^f \left(\theta_{k,l}^L \left(x_k^c, \varphi_k \right) \right) x_k^f + \bar{e}_{k,l} \\ &= \underbrace{x_k^c + \mu_s \tilde{H}_l \left(x_k^c, \varphi_k \right) x_k^f}_{\tilde{h}_{k,l} \left(x_k \right)} + \underbrace{\left(s_{k,l} - \mu_s \right) \tilde{H}_l \left(x_k^c, \varphi_k \right) x_k^f}_{\tilde{e}_{k,l}} + \bar{e}_{k,l} \\ &= \tilde{h}_{k,l} \left(x_k \right) + \tilde{e}_{k,l} \end{aligned} \quad (29)$$

with:

$$\tilde{H}_l \left(x_k^c, \varphi_k \right) = p_{k,l} \left(x_k^c \right) H^f \left(\theta_{k,l}^L \left(x_k^c, \varphi_k \right) \right) \quad (30)$$

$$\tilde{R}_{k,l} = R_{k,l} + \sigma_s^2 \tilde{H}_{k,l} x_k^f \left(x_k^f \right)^T \tilde{H}_{k,l}^T \quad (31)$$

$$R_{k,l} = p_{k,l} R^f \left(\theta_{k,l}^L \left(x_k^c, \varphi_k \right) \right) p_{k,l}^T + R \quad (32)$$

$$\tilde{H}_{k,l} = \tilde{H}_l \left(x_k^c, \varphi_k \right) \quad (33)$$

$$p_{k,l} = s_{k,l} p_{k,l} \left(x_k^c \right) \quad (34)$$

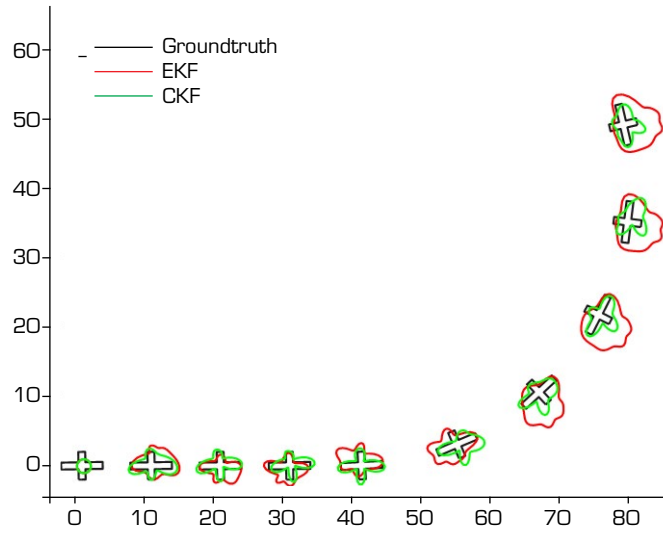
In EOT algorithms relying on GP, the existence of outliers and abrupt object maneuvers may result in non-Gaussian noise exhibiting pronounced heavy-tailed characteristics, which diverge from a Gaussian distribution. Hence, in practical scenarios, it is imperative to account for the impact of non-Gaussian noise. In this paper, following the approach described in (Izanloo *et al.* 2016), w_k and e_k were modeled as zero-mean non-Gaussian noises with a Gaussian mixture distribution. Specifically, the noise is modeled as a mixture of two zero-mean Gaussians, where the outliers are represented by a zero-mean Gaussian with a large covariance, and the distribution function is:

$$f(x) \sim \beta N(\mu_1, P_1) + (1 - \beta) N(\mu_2, P_2) \quad (35)$$

where $0 \leq \beta < 1$ represents the probability of outlier observation, $N(\mu_1, P_1)$ represents Gaussian noise with mean μ_1 and variance P_1 , and $N(\mu_2, P_2)$ represents Gaussian noise with large variance.

Traditional Kalman filters operate on the principle of minimizing mean square error, and their filtering efficacy may degrade in non-Gaussian conditions (Liu *et al.* 2019), consequently diminishing the tracking accuracy of the algorithm. The example depicted in Fig. 3 demonstrates that the utilization of traditional Kalman filtering can result in the failure of EOT based on the GP model in the presence of non-Gaussian noise. Consequently, within the GP model framework, this paper introduces an SRCKF based on MCC in this paper to tackle the EOT challenge amidst a non-Gaussian noise environment.





Source: Elaborated by the authors.

Figure 3. EOT under non-Gaussian noise.

Maximum correntropy criterion-square root cubature Kalman filter (MCC-SRCKF) based on GP

The framework for filtering in object tracking mainly consists of two parts: the object state transition and the sensor measurements generation. Based on the derivation in the extended object model under Gaussian process regression section, the state space model is formulated as follows:

$$\begin{aligned} x_k &= F_k x_{k-1} + w_k \\ z_k &= h_k(x_k) + e_k \end{aligned} \quad (36)$$

where $x_k \in R^n$ represents the system state vector at time k and n is the system state dimension, $z_k \in R^m$ represents the system measurement vector at time k , and m is the measurement dimension. w_k and e_k are the mutually independent system process noise and measurement noise with covariance matrices Q_k and R_k . In this paper, w_k and e_k are modeled as zero mean non-Gaussian noise with a mixed Gaussian distribution.

Standard SRCKF

The heart of the CKF is the third-degree spherical-radial cubature rule, which provides a set of cubature points that scale linearly with the dimension of the state vector. Consequently, the CKF serves as an effective method for high-dimensional nonlinear filtering problems. To ensure both the positive definiteness and symmetry of the error covariance matrix, the SRCKF is introduced. Similar to the standard CKF method, the SRCKF likewise consists of two essential procedures: the time update and the measurement update.

Initialize

Set the initial value $\hat{x}_{0|0}$ of the state and the square-root factor $S_{0|0}$ of the corresponding error covariance matrix. The formula of $S_{0|0}$ is:

$$S_{0|0} = \sqrt{P_{0|0}} \quad (37)$$

where $P_{0|0}$ denotes the error covariance matrix.

Time update

Step 1: calculate the predicted cubature point $X_{k-1|k-1}^i$ and propagate them based on the state transition function:

$$\begin{aligned} X_{k-1|k-1}^i &= \hat{x}_{k-1|k-1} + S_{k-1|k-1} \xi_i, \quad i = 1, 2, \dots, 2n \\ X_{k|k-1}^{i*} &= f(X_{k-1|k-1}^i) \end{aligned} \quad (38)$$

where ξ_i is the set of cubature points, defined as:

$$\xi_i = \begin{cases} \sqrt{n} [1]_i, & i = 1, 2, \dots, n \\ -\sqrt{n} [1]_{i-n}, & i = n+1, \dots, 2n \end{cases} \quad (39)$$

where $[1]_i$ represents the i -th column vector of the identity matrix I of $n \times n$, and n represents the dimension of the state variable.

Step 2: calculate the predicted value of the state $\hat{x}_{k|k-1}$ and the square-root factor of its error covariance matrix $S_{k|k-1}$:

$$\begin{aligned} \hat{x}_{k|k-1} &= \frac{1}{2n} \sum_{i=1}^{2n} X_{k|k-1}^{i*} \\ S_{k|k-1} &= \text{Tri}a\left(\left[X_{k|k-1}^*, \sqrt{Q_{k-1}}\right]\right) \end{aligned} \quad (40)$$

where $\text{Tri}a(\cdot)$ represents QR decomposition and returns a lower triangular matrix. The weighted center matrix $X_{k|k-1}^*$ is defined as follows:

$$X_{k|k-1}^* = \frac{1}{2n} \left[X_{k|k-1}^{1*} - \hat{x}_{k|k-1}, X_{k|k-1}^{2*} - \hat{x}_{k|k-1}, \dots, X_{k|k-1}^{2n*} - \hat{x}_{k|k-1} \right] \quad (41)$$

Measurement update

Step 1: update the cubature points $X_{k|k-1}^i$ and propagate them through the measurement function:

$$\begin{aligned} X_{k|k-1}^i &= \hat{x}_{k|k-1} + S_{k|k-1} \xi_i, \quad i = 1, 2, \dots, 2n \\ Z_{k|k-1}^i &= h(X_{k|k-1}^i) \end{aligned} \quad (42)$$

Step 2: calculate the predicted measurement $\hat{z}_{k|k-1}$ and the square-root factor of its error covariance matrix $S_{k|k-1}^{zz}$:

$$\begin{aligned} \hat{z}_{k|k-1} &= \frac{1}{2n} \sum_{i=1}^{2n} Z_{k|k-1}^i \\ S_{k|k-1}^{zz} &= \text{Tri}a\left(\left[Z_{k|k-1}, \sqrt{R_k}\right]\right) \end{aligned} \quad (43)$$

The weighted central matrix $Z_{k|k-1}$ is defined as follows:

$$Z_{k|k-1} = \frac{1}{2n} \left[Z_{k|k-1}^1 - \hat{z}_{k|k-1}, Z_{k|k-1}^2 - \hat{z}_{k|k-1}, \dots, Z_{k|k-1}^{2n} - \hat{z}_{k|k-1} \right] \quad (44)$$



Step 3: calculate the measurement covariance matrix and the cross-covariance matrix:

$$\begin{aligned} P_{k|k-1}^{zz} &= S_{k|k-1}^{zz} \left(S_{k|k-1}^{zz} \right)^T \\ P_{k|k-1}^{xz} &= X_{k|k-1} Z_{k|k-1}^T \end{aligned} \quad (45)$$

The weighted central matrix $X_{k|k-1}$ is defined as follows:

$$X_{k|k-1} = \frac{1}{2n} \left[X_{k|k-1}^1 - \hat{x}_{k|k-1}, X_{k|k-1}^2 - x_{k|k-1}, \dots, X_{k|k-1}^{2n} - x_{k|k-1} \right] \quad (46)$$

Step 4: obtain the Kalman gain matrix:

$$K_k = P_{k|k-1}^{xz} \left(P_{k|k-1}^{zz} \right)^{-1} \quad (47)$$

Step 5: update the state variable and the square-root factor of the error covariance matrix:

$$\begin{aligned} \hat{x}_{k|k} &= x_{k|k-1} + K_k \left(z_k - \hat{z}_{k|k-1} \right) \\ S_{k|k} &= \text{Triu} \left[X_{k|k-1} - K_k Z_{k|k-1}, \sqrt{R_k} \right] \end{aligned} \quad (48)$$

Square root cubature Kalman filter (SRCKF) algorithm based on MCC

Correntropy represents a novel approach used to quantify the similarity between two random variables. It captures not only second-order information but also higher-order moments of the joint PDF (Cinar and Príncipe 2012). This method has been extensively employed in the processing of non-Gaussian noise signals. For the given random variables X and Y , the correntropy can be expressed using the mathematical expectation of a positive definite kernel function $k_\sigma(X, Y)$:

$$V(X, Y) = E \left[k_\sigma(X, Y) \right] = \iint k_\sigma(x, y) F_{X,Y}(x, y) dx dy \quad (49)$$

where $F_{X,Y}(x, y)$ is the joint PDF between two random variables. In practical applications, the joint PDF is usually unknown and only a limited number of data samples $\{x, y\}$ are available. In this case, the correntropy is often approximated to (Mandanas and Kotropoulos 2016):

$$\hat{V}(X, Y) = \frac{1}{N} \sum_{i=1}^N k_\sigma(x_i, y_i) \quad (50)$$

where $\{x_i, y_i\}_{i=1}^N$ is the N data points sampled from $F_{X,Y}(x, y)$, $k_\sigma(x_i, y_i)$ denotes the Mercer kernel function. In this study, the most popular Gaussian kernel function was used, which is defined as follows:

$$k_\sigma(x_i, y_i) = G_\sigma(e) = \exp \left(-\frac{e^2}{2\sigma^2} \right) \quad (51)$$

where $e = x_i - y_i$, $\sigma > 0$ is the kernel width of correntropy. Using Taylor series to expand the Gaussian kernel shown in Eq. 50 and apply it to Eq. 48, one can obtain the estimator of correntropy as:

$$\hat{V}(X, Y) = \frac{1}{\sqrt{2\pi\sigma}} \sum_{n=0}^{\infty} \frac{(-1)^n}{2^n \sigma^{2n} n!} E \left[(X - Y)^{2n} \right] \quad (52)$$

According to Eq. 51, it is evident that correntropy encompasses information pertaining to all even moments of the random variable $X - Y$. This enables effectively harnessing of high-order moment information from the signal, which forms the primary advantage of utilizing correntropy to mitigate non-Gaussian noise.

The MCC is incorporated into the system. The prediction steps of the MCC-SRCKF mirror those of standard SRCKF. First, the coefficient matrix of \bar{H}_k statistically linearized observation vector, \bar{R}_k is defined, where the estimated covariance matrix of observation noise, and their calculation method is as follows:

$$\bar{H}_k = (P_{k|k-1}^{xz})^T S_{k|k-1}^{-1} \quad (53)$$

$$\bar{R}_k = S_{k|k-1}^{zz} - \bar{H}_k S_{k|k-1} \bar{H}_k^T \quad (54)$$

The objective function is defined by combining the MCC and weighted least squares (WLS) methods:

$$J_{MCC} = G_\sigma \left(\|x_k - \hat{x}_{k|k-1}\|_{S_{k|k-1}^{-1}} \right) + G_\sigma \left(\|z_k - \hat{z}_{k|k-1}\|_{\bar{R}_k^{-1}} \right) \quad (55)$$

To minimize the objective function, its derivative is computed with respect to x_k :

$$\begin{aligned} \frac{\partial J_{MCC}}{\partial x_k} &= \frac{1}{\sigma^2} G_\sigma \left(\|x_k - \hat{x}_{k|k-1}\|_{S_{k|k-1}^{-1}} \right) S_{k|k-1}^{-1} (x_k - x_{k|k-1}) \\ &- \frac{1}{\sigma^2} G_\sigma \left(\|z_k - \hat{z}_{k|k-1}\|_{\bar{R}_k^{-1}} \right) \bar{H}_k^T \bar{R}_k^{-1} (z_k - z_{k|k-1}) = 0 \end{aligned} \quad (56)$$

$$S_{k|k-1}^{-1} x_k - S_{k|k-1}^{-1} F \hat{x}_{k|k-1} = G_k \bar{H}_k^T \bar{R}_k^{-1} (z_k - \hat{z}_{k|k-1}) \quad (57)$$

where:

$$G_k = \frac{G_\sigma \left(\|z_k - \hat{z}_{k|k-1}\|_{\bar{R}_k^{-1}} \right)}{G_\sigma \left(\|x_k - \hat{x}_{k|k-1}\|_{S_{k|k-1}^{-1}} \right)} \quad (58)$$

Then, the new estimator is derived from Eq. 55 as follows:

$$\hat{x}_{k|k} = x_{k|k-1} + \bar{K}_k (z_k - \hat{z}_{k|k-1}) \quad (59)$$

$$\bar{K}_k = G_k S_{k|k-1} \bar{H}_k^T (\bar{R}_k + G_k \bar{H}_k S_{k|k-1} \bar{H}_k^T)^{-1} \quad (60)$$

The update of the error covariance matrix can be calculated by the following equation:

$$P_{k|k} = (I - \bar{K}_k \bar{H}_k) S_{k|k-1} \quad (61)$$

The process of the GP-MCC-SRCKF algorithm is shown in Fig. 4.

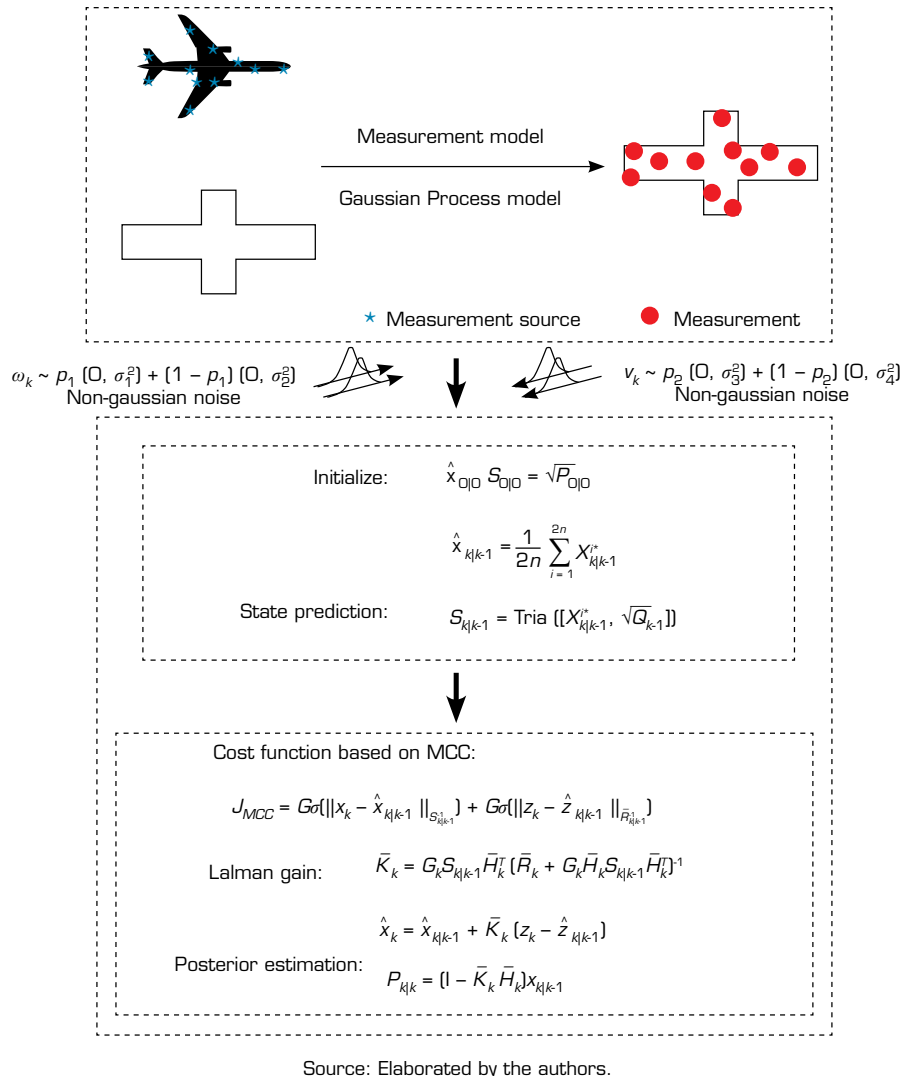


Figure 4. Flow chart of the GP-MCC-SRCKF algorithm.

The traditional KF is formulated based on the minimum mean square error criterion, which is optimal when Gaussian assumptions hold. However, filtering performance degrades when the system is subject to non-Gaussian noise. MCC can capture both second-order and higher-order moments of error signals. In this section, MCC is combined with SRCKF to develop an EOT filtering algorithm using GP regression to address non-Gaussian noise environments.

SIMULATION RESULTS

To validate the tracking performance of the proposed algorithm, separate simulation experiments were conducted in two different scenarios in this section. Additionally, the proposed algorithm was compared with GP-EKF and GP-CKF, and a detailed analysis of both the extended object contour estimation and object kinematic state was performed. Regarding the object contour estimation, evaluation was conducted using intersection over union (IOU) and Hausdorff distance. For the kinematic state, the commonly used root mean squared error (RMSE) was employed for evaluation. A total of 100 Monte Carlo simulation experiments were conducted for each simulated scenario, and the presented results depict the average values across all iterations.

Algorithm performance evaluation indicators

Root mean squared error (RMSE)

The performance of the object position and velocity was evaluated using RMSE:

$$RMSE(x, \hat{x}) = \sqrt{\frac{1}{N} \sum_{k=1}^N (x_k - \hat{x}_k)^2} \quad (62)$$

where x and \hat{x} represent the true value and the estimated value, respectively. The smaller the RMSE value, the closer the estimated shape of the corresponding algorithm is to the true extended shape of the object.

Intersection over union (IOU) and Hausdorff distance

The performance of the object extent estimation was evaluated based on the IOU measure and Hausdorff distance, assuming that R_0 and \hat{R} are the true shape and the estimated shape, respectively.

IOU is defined as the area ratio of the intersection and union of these two regions, calculated as follows:

$$IOU(\hat{R}, R_0) = \frac{area(\hat{R} \cap R_0)}{area(\hat{R} \cup R_0)} \quad (63)$$

where $area(\cdot)$ represents the calculation area. $IOU(\hat{R}, R_0) \in [0, 1]$, when $IOU(\hat{R}, R_0) = 1$, indicates that the estimated shape and the real shape completely coincide, when $IOU(\hat{R}, R_0) = 0$, the estimated shape and the real shape have no intersection, that is, the regions do not even overlap.

The Hausdorff distance serves as an indicator to measure the performance of extended form estimation in the process of EOT. A smaller value indicates that the shape estimated by the corresponding algorithm is closer to the true extended form of the object. The calculation method is as follows:

$$d_H[R_0, \hat{R}] = \max\{d(R_0, \hat{R}), d(\hat{R}, R_0)\} \quad (64)$$

Experimental analysis

Scenario A

For this experiment, a cross-shaped object with a long axis of 6 m and a short axis of 4 m was selected. The object shape was rigid. The initial kinematic state is $\bar{x}_1 = [0, 0, \pi/2, 1, 1, 0]^T$, and the extent state is a fifty-dimensional vector with all values set to 1. The true trajectory of the object comprises a combination of constant velocity (CV) and constant turn (CT) models. The real motion model of the object is illustrated in Table 1.

Table 1. Object real motion model.

Simulation step	(0,40)	(40,130)	(130,220)	(22,260)	(260,300)
Turning rate (rad-s)	0	1	-1	0	1

Source: Elaborated by the authors.

The kinematic state transition matrices and the covariance matrix of process noise are:

$$\bar{F} = \begin{bmatrix} 1 & T \\ 0 & 1 \end{bmatrix} \otimes I_3 \quad (65)$$

$$\bar{Q}_k = \begin{bmatrix} \frac{T^3}{3} & \frac{T^2}{2} \\ \frac{T^2}{2} & T \end{bmatrix} \otimes \begin{bmatrix} \sigma_q^2 & 0 & 0 \\ 0 & \sigma_q^2 & 0 \\ 0 & 0 & \sigma_\varphi^2 \end{bmatrix} \quad (66)$$

where \otimes is the Kronecker product. The process noise variances of object position and direction are $\sigma_q = 10^{-2}$ and $\sigma_\varphi = 10^{-3}$, respectively, and $\alpha = 10^{-2}$ has been used for the object extent dynamics. The parameters of the covariance function of GP are $\sigma_r = 2$, $\sigma_f = 0.8$, $l = \pi / 4$. The measurements are uniformly distributed over the object surface, with 20 measurements generated per scan. The covariance of sensor noise is $R = 10^{-2} I_2$, and the sampling time has been set to $T = 1s$.

To validate the effectiveness of the proposed strategy in object tracking under non-Gaussian conditions, the following experiment was conducted. For this experiment, both the process noise and measurement noise were assumed to be heavy-tailed non-Gaussian noises following a mixture Gaussian distribution:

$$\begin{aligned} w_k &\sim \beta N(0, Q_k) + (1-\beta) N(0, 50Q_k) \\ e_k &\sim \beta N(0, R_k) + (1-\beta) N(0, 50R_k) \end{aligned} \quad (67)$$

where $\beta=0.7$ is set in this paper.

In the aforementioned simulation scenario, the traditional GP-EKF and GP-CKF were compared with the GP-MCC-SRCKF proposed in this paper. Figures 4 and 5 and Table 2 illustrate the estimation performance of the three algorithms. The smaller the values of RMSE and Hausdorff distance, the higher the estimation accuracy of the algorithm. Conversely, the larger the IOU value, the higher the accuracy of the algorithm.

To facilitate comparison of results from different methods, data with the highest accuracy are in bold.

Upon observing the object motion trajectory depicted in Fig. 5, it becomes apparent that from approximately 40 steps onwards, the original object tracking algorithm GP-EKF experiences a significant divergence in shape, with the estimated results deviating substantially from the true shape. While GP-CKF exhibits greater accuracy in comparison to others, its stability remains uncertain, potentially leading to sudden divergences during shape estimation. Data analysis confirms that as a result of the drastic changes in the object state during turning, the likelihood of sensor data producing outliers rises, with non-Gaussian noise becoming more prominent, resulting in an increase in errors for GP-EKF and GP-CKF. Consequently, after 80 steps, the original algorithm is no longer able to complete the entire tracking process. The proposed method consistently maintains high performance in position tracking and shape estimation, embodying the advantages of the MCC algorithm in dealing with non-Gaussian noise problems.

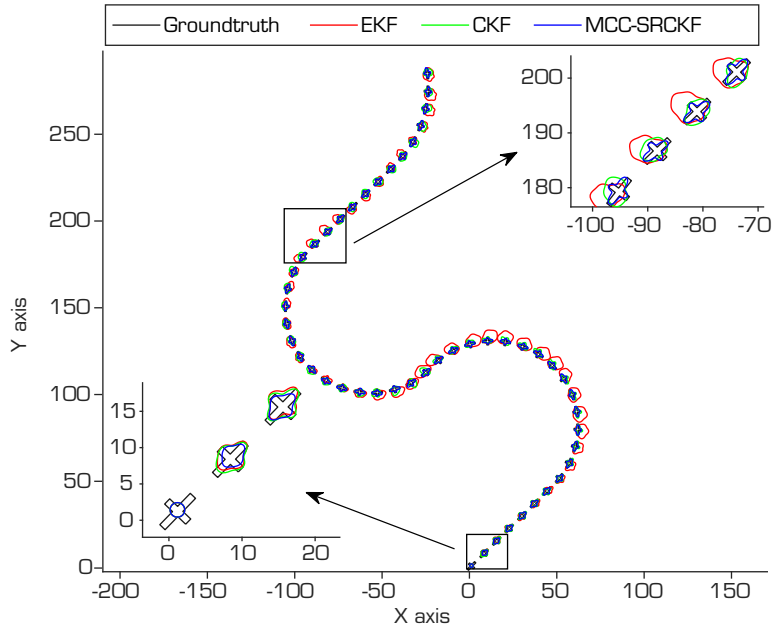
From Table 3, it can be seen that, compared with other methods, their algorithm is closest to the real value and can accurately estimate the orientation of the object.

To facilitate comparison of results from different methods, data with the highest accuracy are in bold.

From Fig. 6a, it can be seen that the RMSE of the proposed algorithm for estimating the centroid position of the extended object is considerably lower than that of the GP-EKF and GP-CKF algorithms, with a reduction of 84 and 37%, respectively. Compared with the GP-EKF and GP-CKF algorithms, the GP-MCC-SRCKF algorithm provides a more accurate estimation of the centroid position of the extended object, enhancing the accuracy of estimating the position of the extended object in non-Gaussian noise environments. In Fig. 6b, the convergence process of the proposed algorithm for estimating the RMSE of the extended object's speed is comparable to that of the GP-EKF and GP-CKF algorithms. These three algorithms demonstrate good performance in estimating the speed of the extended object, all of which can effectively estimate the speed of the extended object with high accuracy.

From Fig. 6c, it can be seen that the tracking accuracy of the proposed algorithm steadily rises during the first 60 steps of motion, subsequently stabilizing between 0.5 and 0.7 after 60 steps. Conversely, the traditional GP-EKF algorithm exhibits significant fluctuations in IOU values and is thus unstable. This observation demonstrates that the algorithm fails to effectively track the object in non-Gaussian noise environments. However, despite the GP-CKF algorithm displaying an upward trend during the initial few seconds, its accuracy rapidly deteriorates in subsequent experimental processes. Similarly, to mitigate the limitations of IOU, the Hausdorff distance was utilized

to further validate the tracking situation. In Fig. 6d, it is evident that, similar to the IOU, the Hausdorff distance values of the GP-EKF and GP-CKF algorithms are unstable and exhibit poor tracking accuracy. However, the proposed algorithm ultimately demonstrates good convergence accuracy, highlighting the advantages of the MCC algorithm in addressing non-Gaussian noise problems.



Source: Elaborated by the authors.

Figure 5. Trajectory of the extended object in scenario A (the black line is for the true object, the red line, green line, and blue line are for EKF, CKF, and MCC-SRCKF, respectively).

Table 3. Comparison of average object orientation angles in scenario A.

	Ground truth	EKF	CKF	MCC-SRCKF
Orientation [degree]	1.79	0.98 [-0.81]	2.79 [+1.00]	1.77 [-0.02]

Source: Elaborated by the authors.

In summary, the proposed algorithm has the potential to significantly enhance estimation accuracy, and effectively suppress divergence in object tracking.

Scenario B

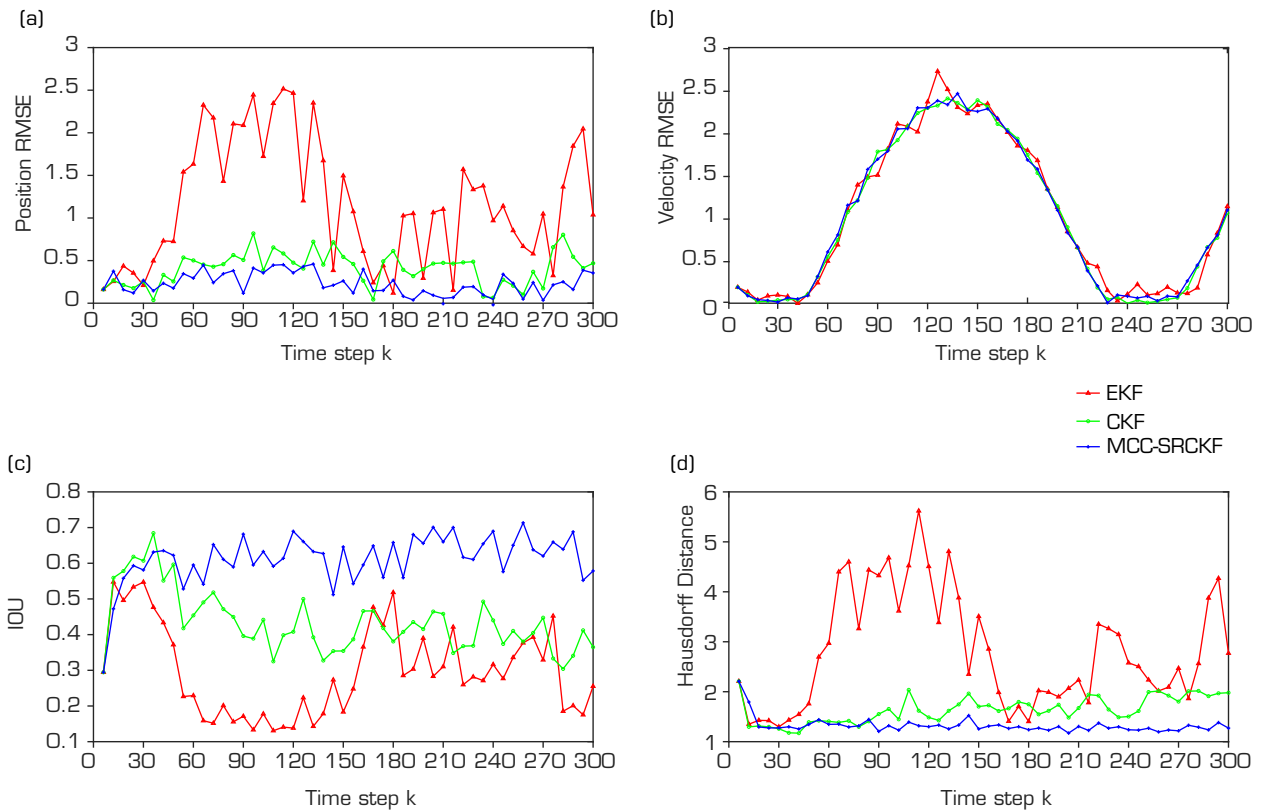
Furthermore, simulation experiments were conducted in another, and more complex turning scenario to further illustrate the applicability and effectiveness of the proposed method across various tracking scenarios. During the entire movement process, the object executes a turn at a turning rate $\pm\pi / 200(\text{rad} / \text{s})$, accompanied by its own rotation throughout the turn. The settings for the initial state and state transition matrix parameters remain consistent with those of scenario A.

Assuming that both the process noise and measurement noise are non-Gaussian noise and follow a mixed Gaussian distribution:

$$\begin{aligned}
 w_k &\sim 0.7N(0, Q_k) + 0.3N(0, 50Q_k) \\
 e_k &\sim 0.7N(0, R_k) + 0.3N(0, 50R_k)
 \end{aligned}
 \tag{68}$$

Likewise, the simulation results of the original algorithm were compared with the algorithm proposed in this paper. Figures 7 and 8 and Table 4 present the performance comparison results for the three algorithms.





Source: Elaborated by the authors.

Figure 6. Performance comparison for scenario A. (a) position RMSE; (b) velocity RMSE; (c) IOU; (d) Hausdorff distance.

From Table 5, it can be seen that under the disturbance of non-Gaussian noise, EKF and CKF exhibit significant errors, while the proposed algorithm can accurately estimate the orientation of the extended object.

To facilitate comparison of results from different methods, data with the highest accuracy are in bold.

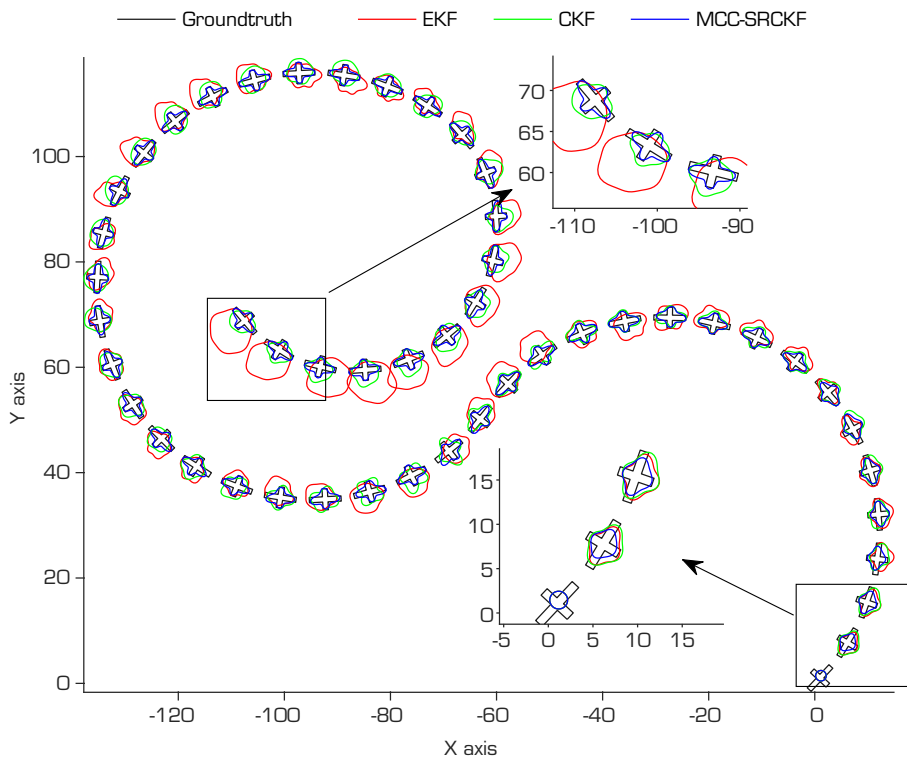
Figure 7 shows the motion trajectory in scenario B. It is clear that when the noise is non-Gaussian, the tracking performance of the original algorithm has already diverged from the beginning of the turn. The main reason is that the EKF and CKF are sensitive to large outliers. In contrast, the algorithm introduced in this paper has better tracking accuracy and is more stable.

The comparison of the RMSE results for centroid position in Fig. 8a reveals that the proposed algorithm in this paper yields the lowest overall RMSE in centroid estimation, indicating a more accurate estimation of the extended object's real-time position under abnormal noise conditions. Figure 8b demonstrates that the proposed algorithm has a comparable estimation error for the extended object's speed relative to the other two algorithms, both of which effectively estimate the extended object's speed with high accuracy. The accuracy of object shape estimation in Fig. 8c and d shows that under non-Gaussian noise conditions, the GP-EKF algorithm experiences significant interference, resulting in considerable fluctuations in the estimation results. Although the GP-CKF algorithm exhibits higher accuracy than the others, its stability is not assured, and it may suddenly diverge during shape estimation. However, when utilizing the MCC, the proposed method demonstrates enhanced resistance to non-Gaussian noise and superior estimation accuracy.

Table 4. Performance comparison results of three algorithms.

	Position RMSE	Velocity RMSE	IOU	Hausdorff distance
GP-EKF	0.59	0.64	0.32	2.45
GP-CKF	0.14	0.63	0.43	1.68
GP-MCC-SRCKF	0.08	0.62	0.63	1.29

Source: Elaborated by the authors.



Source: Elaborated by the authors.

Figure 7. Trajectory of the extended object in scenario B (the black line is for the true object, the red line, green line, and blue line are for EKF, CKF, and MCC-SRCKF, respectively).

Table 2. Performance comparison results of the three algorithms.

	Position RMSE	Velocity RMSE	IOU	Hausdorff distance
GP-EKF	0.72	0.89	0.3	2.81
GP-CKF	0.19	0.89	0.43	1.64
GP-MCC-SRCKF	0.12	0.88	0.61	1.19

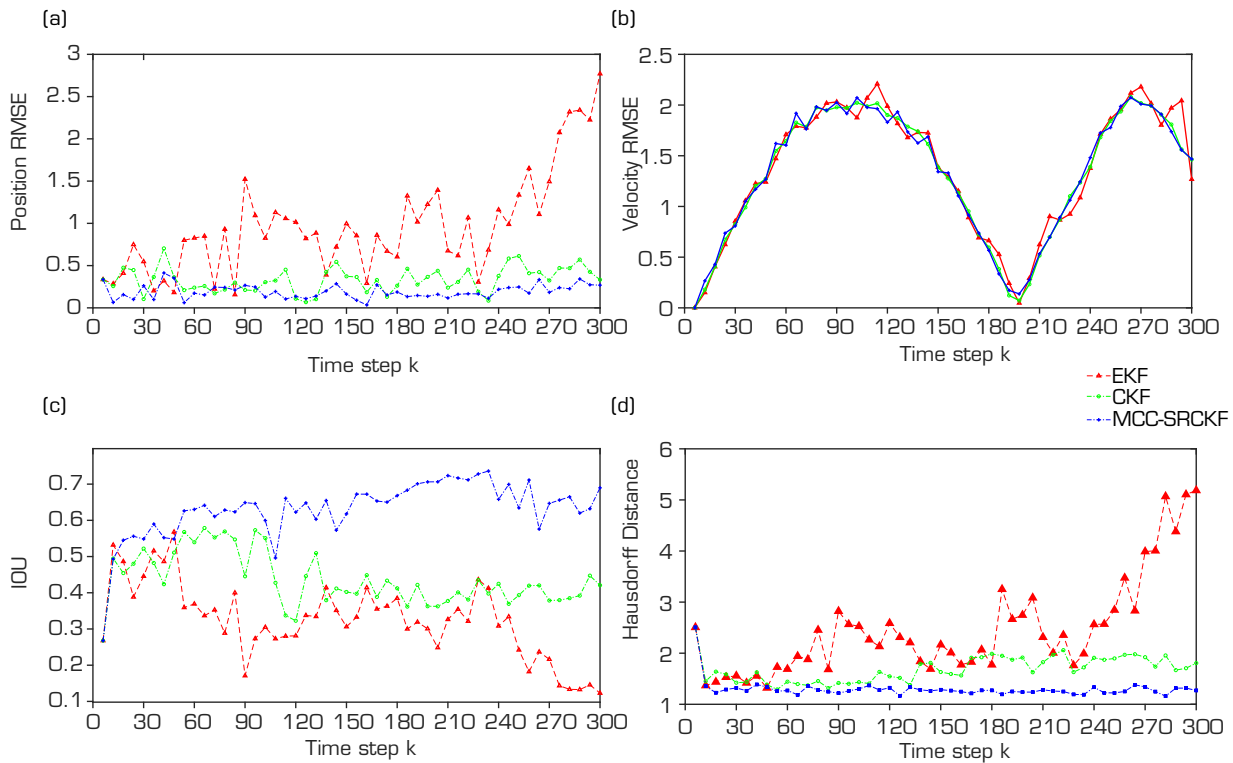
Source: Elaborated by the authors.

CONCLUSION

In this paper, the GP-MCC-SRCKF algorithm was proposed to accurately estimate the state of extended objects in the presence of non-Gaussian noise. The proposed method utilizes GP to model object extent and estimate kinematic state, while the MCC is employed to address non-Gaussian noise. Simulation results demonstrated that the proposed algorithm outperforms traditional methods in accurately estimating the kinematic state and contour state of extended objects, especially in environments with non-Gaussian noise interference.

Although the MCC-SRCKF algorithm achieves good performance, the choice of kernel width in the correlation entropy criterion is crucial to reduce the influence of outliers. As future work, optimizing the kernel width size using adaptive mechanisms, such as particle swarm optimization, will be pursued to ensure that the error covariance of the filter is minimized.





Source: Elaborated by the authors.

Figure 8. Performance comparison for scenario B. (a) position RMSE; (b) velocity RMSE; (c) IOU; (d) Hausdorff distance.

Table 5. Comparison of average object orientation angles in scenario B.

	Ground truth	EKF	CKF	MCC-SRCKF
Orientation (degree)	1.02	3.63 (+2.61)	2.42 (+1.40)	0.78 (-0.24)

Source: Elaborated by the authors.

CONFLICT OF INTEREST

Nothing to declare.

AUTHORS' CONTRIBUTION

Conceptualization: Sun L; **Data curation:** Sun L and Wang Y; **Formal analysis:** Sun L; **Acquisition of funding:** Sun L; **Research:** Sun L and Wang Y; **Methodology:** Sun L; **Project administration:** Wang Y and Gao D; **Resources:** Sun L and Gao D; **Software:** Sun L and Wang Y; **Supervision:** Sun L and Gao D; **Validation:** Sun L and Wang Y; **Visualization:** Not applicable; **Writing - Preparation of original draft:** Sun L and Wang Y; **Writing - Proofreading and editing:** Sun L and Wang Y; **Final approval:** Sun L.

DATA AVAILABILITY STATEMENT

Data sharing is not applicable.

FUNDING

National Natural Science Foundation of China 

Grant No: 62271193

Major Science and Technology Projects of Longmen Laboratory

Grant No: 231100220300

Key Research and Development and Promotion of Special (Science and Technology) Project of Henan Province, China

Grant No: 242102211031

Key Scientific Research Project of Higher Education Institutions in Henan Province, China

Grant No: 24B520010

Frontier Exploration Project of Longmen Laboratory, China

Grant No: LMQYTSKT034

ACKNOWLEDGMENTS

Not applicable.

REFERENCES

- Aftab W, Hostettler R, De Freitas A, Arvaneh M, Mihaylova L (2019) Spatio-temporal Gaussian process models for extended and group object tracking with irregular shapes. *IEEE Trans Veh Technol* 68(3):2137-2151. <https://eprints.whiterose.ac.uk/140444/>
- Baum M, Hanebeck UD (2012) Extended object tracking based on set-theoretic and stochastic fusion. *IEEE Trans Aerosp Electron Syst* 48(4):3103-3115. <https://doi.org/10.1109/TAES.2012.6324680>
- Baum M, Hanebeck UD (2014) Extended object tracking with random hypersurface models. *IEEE Trans Aerosp Electron Syst* 50(1):149-159. <https://doi.org/10.1109/TAES.2013.120107>
- Chen B, Liu X, Zhao H, Principe C (2017) Maximum correntropy Kalman filter. *Automatica* 76:70-77. <https://doi.org/10.1016/j.automatica.2016.10.004>
- Cinar GT, Príncipe JC (2012) Hidden state estimation using the correntropy filter with fixed point update and adaptive kernel size. Paper presented 2012 International Joint Conference on Neural Networks. IEEE; Brisbane, Australia.
- Ebert F, Wuensche HJ (2019) Dynamic object tracking and 3D surface estimation using Gaussian processes and extended Kalman filter. Paper presented 22nd IEEE Intelligent Transportation Systems Conference. IEEE; Auckland, New-Zealand. <https://doi.org/10.1109/ITSC.2019.8916891>
- Feldmann M, Fränken D, Koch W (2010) Tracking of extended objects and group targets using random matrices. *IEEE Trans Signal Process* 59(4):1409-1420. <https://doi.org/10.1109/TSP.2010.2101064>
- Feldmann M, Koch W (2012) Bayesian approach to extended object and cluster tracking using random matrices. *IEEE Trans*



- Aerosp Electron Syst 48(2):1687-1693. <https://doi.org/10.1109/TAES.2008.4655362>
- Granström K, Baum M, Reuter S (2017) Extended object tracking: introduction, overview, and applications. *J Adv Inf Fusion* 12(2):139-174. <https://doi.org/10.48550/arXiv.1604.00970>
- Guo Y, Li Y, Tharmarasa R, Kirubarajan T, Efe M, Sarikaya B (2018) GP-PDA filter for extended target tracking with measurement origin uncertainty. *IEEE Trans Aerosp Electron Syst* 55(4):1725-1742. <https://doi.org/10.1109/TAES.2018.2875555>
- Hirscher T, Scheel A, Reuter S, Dietmayer K (2016) Multiple extended object tracking using Gaussian processes. Paper presented 2016 19th International Conference on Information Fusion. IEEE; Heidelberg, Germany.
- Izanloo R, Fakoorian SA, Yazdi HS, Simon D (2016) Kalman filtering based on the maximum correntropy criterion in the presence of non-Gaussian noise. Paper presented 2016 IEEE National Aerospace and Electronics Conference. IEEE; Dayton, USA. <https://doi.org/10.1109/CISS.2016.7460553>
- Koch JW (2008) Bayesian approach to extended object and cluster tracking using random matrices. *IEEE Trans Aerosp Electron Syst* 44(3):1042-1059. <https://doi.org/10.1109/TAES.2008.4655362>
- Kumru M, Özkan E (2018) 3D extended object tracking using recursive Gaussian processes. Paper presented 2018 21st International Conference on Information Fusion. IEEE; Cambridge, UK. <https://doi.org/10.23919/ICIF.2018.8455480>
- Kumru M, Özkan E (2021) Three-dimensional extended object tracking and shape learning using Gaussian processes. *IEEE Trans Aerosp Electron Syst* 57(5):2795-2814. <https://doi.org/10.1109/TAES.2021.3067668>
- Kunz F, Nuss D, Wiest J, Deusch H, Reuter S, Gritschneider F, Scheel A, Stübler M, Bach M, Hatzelmann P *et al.* (2015) Autonomous driving at Ulm University: A modular, robust, and sensor-independent fusion approach. Paper presented 2015 IEEE intelligent vehicles symposium, IEEE; Seoul, Korea (South) <https://doi.org/10.1109/IVS.2015.7225761>
- Lan J, Li XR (2014) Tracking of maneuvering non-ellipsoidal extended object or target group using random matrix. *IEEE Trans Signal Process* 62(9):2450-2463. <https://doi.org/10.1109/TSP.2014.2309561>
- Liu W, Pokharel PP, Principe JC (2007) Correntropy: properties and applications in non-Gaussian signal processing. *IEEE Trans Signal Process* 55(11):5286-5298. <https://doi.org/10.1109/TSP.2007.896065>
- Liu X, Ren Z, Lyu H, Jiang Z, Ren P, Chen B (2019) Linear and nonlinear regression-based maximum correntropy extended Kalman filtering. *IEEE Trans Syst Man Cybern: Systems* 51(5):3093-3102. <https://doi.org/10.1109/TSMC.2019.2917712>
- Lv S, Zhao H, Zhou L (2021) Maximum mixture total correntropy adaptive filtering against impulsive noises. *Signal Process* 189:108236. <https://doi.org/10.1016/j.sigpro.2021.108236>
- Mandanas FD, Kotropoulos CL (2016) Robust multidimensional scaling using a maximum correntropy criterion. *IEEE Trans Signal Process* 65(4):919-932. <https://doi.org/10.1109/TSP.2016.2625265>
- Osborne M, Osborne MA (2010) Bayesian Gaussian processes for sequential prediction, optimisation and quadrature (doctoral dissertation). Oxford: Oxford University.
- Sun L, Lan J, Li XR (2012) Extended target tracking using star-convex model with nonlinear inequality constraints. Paper presented 2012 31st Chinese Control Conference. IEEE; Hefei, China.
- Sun L, Zhang J, Yu H, Fu Z, He Z (2022) Maneuvering extended object tracking with modified star-convex random hypersurface model based on minimum cosine distance. *Remote Sens* 14(17):4376. <https://doi.org/10.3390/rs14174376>
- Thormann K, Baum M, Honer J (2018) Extended target tracking using Gaussian processes with high-resolution automotive

radar. Paper presented 2018 21st International Conference on Information Fusion. IEEE; Cambridge, UK. <https://doi.org/10.23919/ICIF.2018.8455630>

Wahlström N, Özkan E (2015) Extended target tracking using Gaussian processes. *IEEE Trans Signal Process* 63(16):4165-4178. <https://doi.org/10.1109/TSP.2015.2424194>

Zhou Y, Wang T, Hu R, Su H, Liu Y, Liu X, Suo J, Snoussi H (2019) Multiple kernelized correlation filters (MKCF) for extended object tracking using X-band marine radar data. *IEEE Trans Signal Process* 67(14):3676-3688. <https://doi.org/10.1109/TSP.2019.2917812>

Zhu H, Zhang G, Li Y, Leung H (2021) A novel robust Kalman filter with unknown non-stationary heavy-tailed noise. *Automatica* 127:109511. <https://doi.org/10.1016/j.automatica.2021.109511>

Zhu H, Zou K, Li Y, Leung H (2020) Robust sensor fusion with heavy-tailed noises. *Signal Process* 175:107659. <https://doi.org/10.1016/j.sigpro.2020.107659>

Zhu J, Wang Z, Zhang L, Zhang W (2019) State and parameter estimation based on a modified particle filter for an in-wheel-motor-drive electric vehicle. *Mech Mach Theory* 133:606-624. <https://doi.org/10.1016/j.mechmachtheory.2018.12.008>

Zong P, Barbary M (2015) Improved multi-Bernoulli filter for extended stealth targets tracking based on sub-random matrices. *IEEE Sens J* 16(5):1428-1447. <https://doi.org/10.1109/JSEN.2015.2499268>